Nonlinear Model Updating of a Cantilevered Plate and a Stiffened Skin Panel from a Lynx Helicopter

Matthew S. Allen[1]
Engineering Physics Department, University of Wisconsin-Madison

Ben Weekes[2]
Mechanical Engineering Department, University of Bristol

This work explores technologies for nonlinear modeling, testing and nonlinear model updating of geometrically nonlinear structures. The methodology centers around a finite element model (FEM) of the structure, created and solved using commercial software. A nonlinear reduced order model (ROM) is extracted from the FEM using the implicit condensation and expansion method and its nonlinear normal modes are computed using a pseudo-arclength continuation algorithm. The nonlinear modes provide insight into the dynamics of the FEM/ROM and also provide a comparison that guides model updating and validation. Measurements from the structure using swept or stepped sine excitation are compared with the nonlinear mode backbones to assess their accuracy. Both structures show deformation shapes that change in specific ways with increasing response amplitude, so full-field measurements would be helpful in understanding how the underlying linear modes of the structure interact as the response amplitude increases. These concepts are illustrated on two structures, a cantilevered flat plate which was used in other works to study crack growth in titanium, and a curved exterior panel from a Lynx helicopter. These structures reveal the potential, as well as the limitations, of the current state of the art in modeling and testing these types of structures.

I. Introduction

GEOMETRIC nonlinearities are often important in thin walled structures whenever the shell displacement becomes an appreciable fraction of the thickness. While it has been possible to model these types of structures in nonlinear finite element codes for a few decades [1], these models are exceedingly expensive to integrate and so they have not been used widely for dynamic analysis or design. Fortunately, considerable progress has been made in recent years to develop methods that extract a reduced order model (ROM) for a geometrically nonlinear structure from a series of static loads or displacements applied to the finite element model [2, 3]. Kuether and Allen recently suggested that the nonlinear normal modes (NNMs) of a structure can be compared between candidate ROMs to evaluate the convergence/accuracy of the ROM, as they provide an amplitude dependent view of the dynamics of the structure (or ROM) that is independent of the loading [4, 5]. They have also presented a method whereby the true NNMs of the finite element model can be computed [6]. Peeters, Kerschen and Golinval recently laid the foundation for measuring the nonlinear normal modes of a lightly damped structure [7], and hence it begins to be appealing to use NNMs as a metric to validate and update a nonlinear structural model.

This work seeks to combine these tools to model and then use tests to update/validate geometrically nonlinear finite element models. The methods are evaluated on two structures. The first is a cantilevered plate that is clamped at its base and exhibits a lightly damped two-stripe mode; this type of mode can be problematic in the compressor blades of some turbine engines. The plate of interest is constructed of titanium and was designed to be used to evaluate life prediction and crack propagation methods [8], and so it is important to have an accurate understanding of the stress field in the part as it undergoes geometrically nonlinear motions. This simple structure was found to exhibit several subtleties which make model updating challenging and shed light on best practices for future studies.

[1] Associate Professor, 535 Engineering Research Building, 1500 Engineering Drive, Madison, WI 53706-1609, USA, msallen@engr.wisc.edu, AIAA Lifetime Member.
[2] Postdoctoral Researcher, Queen's Building, University Walk, BS8 1TR, UK, B.Weekes@Bristol.ac.uk

For the second case we seek to probe the limits of these technologies by tackling a more complicated structure with many uncertain parameters. The structure is a panel from a Lynx Helicopter, similar to the one shown in Fig. 1, which is currently housed in the laboratory at the University of Bristol. The panel was removed from the underside of the vehicle and is constructed from fiberglass. The material properties are unknown as is the weave of the glass fibers and the panel incorporates a stiffener with a light weight (probably honeycomb) core and a fiberglass skin. Hence, there are several parameters that will require updating even though the geometry is fairly simple. The authors are not privy to any information regarding the loadings on this panel, so we do not know whether it behaved nonlinearly in flight; it was chosen simply because it was simple enough to model with reasonable effort, yet also more complicated than any structure that has previously been addressed with the proposed tools. Hence, this effort is expected to provide insight into how these tools will perform in an industrial setting and to highlight areas where further research is needed.

(Public domain photo, credit: http://en.wikipedia.org/wiki/File:Lynx_helo_2.jpg)

Figure 1. Photograph of the Lynx helicopter (top) and front (bottom-left) and back (bottom-right) views of the panel that was studied, suspended by bungee cords for a free-free test.

II. Model Updating Approach

The basic approach employed in this work is summarized below and in Fig 2.

1. Create and mesh an FEA model.
2. Perform a low-level (linear) modal test to estimate the natural frequencies and mode shapes.
3. Compare test and FEA model and update material properties and/or section thicknesses until linear modal parameters agree for all modes in the frequency range of interest.
4. Perform swept sine tests to identify those modes that are most susceptible to nonlinearity.
5. Perform stepped-sine or swept-sine tests near the peaks for the modes of interest:
    a. Extract the point at which the response is 90 degrees out of phase with the force [7, 9].
    b. Repeat at various force levels to and combine to construct the NNM backbone.
6. Create a ROM from the finite element model.
    a. Select the modes to include in the ROM.

b. Select the forcing levels to use to estimate the ROM coefficients.

7. Compute the NNMs from the ROM and compare with measurements. Iterate on step (6) and on steps (1) and (3) until the ROM NNMs agree with those measured experimentally.

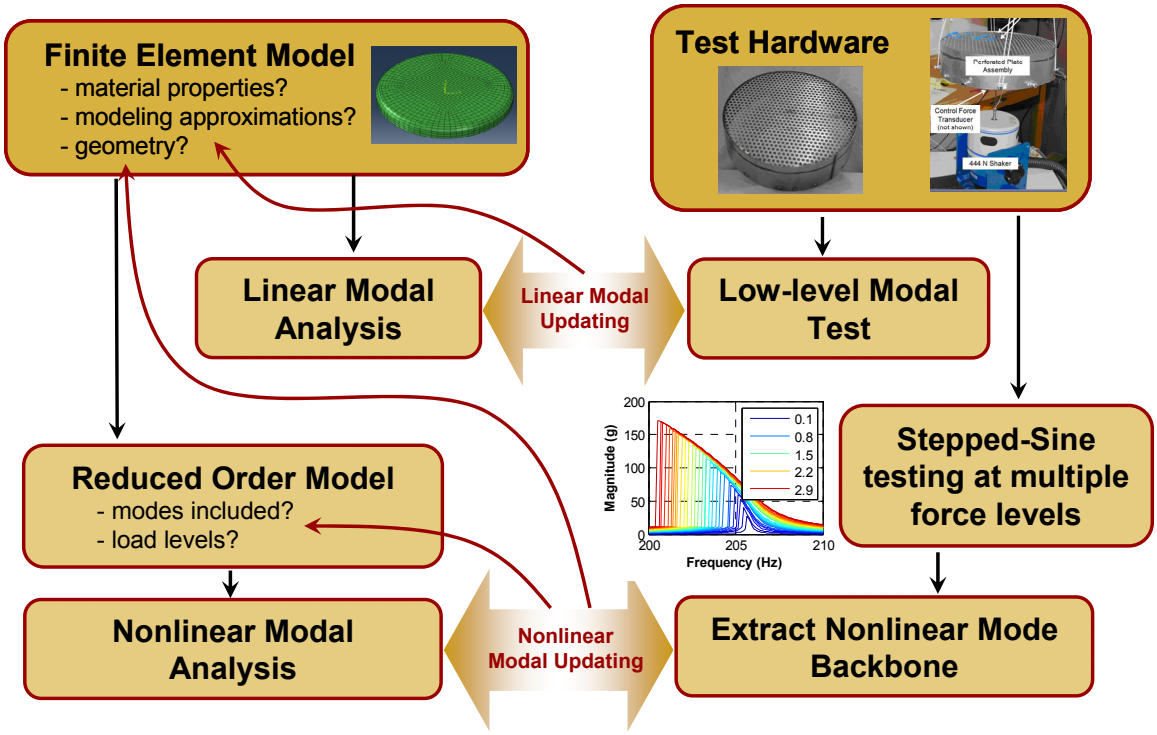

Figure 2. Schematic of the proposed nonlinear model updating procedure.

At a minimum one can compare the nonlinear normal mode frequencies of the model to those measured experimentally. When full-field measurements are available, this comparison can be further informed by considering how the deformation shapes of the structure change with forcing amplitude. To explore this, for the Lynx helicopter panel a scanning laser Doppler vibrometer (LDV) was used to acquire measurements. These measurements were found to provide important insights to guide step (7).

The reduced order modeling theory is explained in several other works [12, 13] and will only be summarized here. The FE model is presumed to be governed by the following equation of motion, where no damping or mass nonlinearities are present.

$$\mathbf{M}\ddot{\mathbf{x}} + \mathbf{K}\mathbf{x} + \mathbf{f}_{NL}(\mathbf{x}) = \mathbf{F}(t) \tag{1}$$

The linear modes transform this equation into the following form, where each modal amplitude is denoted q_r.

$$\ddot{q}_r + \omega_r^2 q_r + \theta_r(q_1, q_2, \ldots, q_N) \approx \boldsymbol{\varphi}_r^T \mathbf{F}(t) \tag{2}$$

The nonlinearities couple the linear modal coordinates through the function θ, which is assumed to have the following form.

$$\theta_r(q_1, q_2, \ldots, q_N) \approx \sum_{i=1}^{N}\sum_{j=i}^{N} B_r(i,j) q_i q_j + \sum_{i=1}^{N}\sum_{j=i}^{N}\sum_{k=j}^{N} A_r(i,j,k) q_i q_j q_k \tag{3}$$

A series of nonlinear static analyses are performed in a commercial FEA package to estimate the coefficients A_r and B_r. This method often produces highly efficient ROMs; sometimes only a single modal coordinate is adequate to describe the structure over a wide range of energy. However, in other cases many more modes must be included.

III. Cantilevered Flat Plate

The finite element model for the first structure of interest is shown in Fig. 3a. The plate is held in a clamp with a curved (sinusoidal) edge in the *x*-*y* plane (this was found to minimize stresses near the clamp and the propensity for cracks to initiate there. The clamp is simulated by adding discrete springs in the out of plane direction between each of the nodes in the region shown in Fig. 3c and ground. The in-plane DOF were left free. The nodes on the bottom edge of the plate were constrained in the *y*-direction and the node on the bottom-left was constrained in *x*- and *y*-.

The mode that will be exercised in the fatigue tests of this structure is shown in Fig. 3b. The stresses are highest in the region near the center of the plate, both due to bending stress and membrane stresses that become important due to geometric nonlinearity. Various design studies were performed prior to the work in [8], and the FE model was found to accurately represent an ensemble of specimens when the nominal material properties shown in Table 1 were used in the FE model. For this work a specific specimen was considered and some limited testing was performed to provide data for model validation. The average density of the specimen was known to be quite accurate and because this and the thickness and modulus all have an almost indistinguishable effect on the natural frequencies, ρ and h were left at their nominal values as the other parameters, Young's modulus, E, and Poisson's ratio, ν, were updated. The specimen is constructed from Titanium, specifically Ti-6AL-2Sn-4Zr-2Mo, duplex annealed and the nominal material properties from MIL-HDBK-5H are shown in Table 1.

Table 1: Parameters of FE model for Cantilevered Plate before and after various updating steps.

Parameter	Initial Values Model t0	Updated Model t1	Updated Model t2
E	16.5 Msi	17.92 Msi	16.77 Msi
ν	0.325	0.291	0.330
ρ	0.164 lb/in^3	unchanged	unchanged
h	0.0511 in ±0.001 in	unchanged	unchanged
k (springs in the clamped region)	2000 lb/in	141 lb/in	625 lb/in

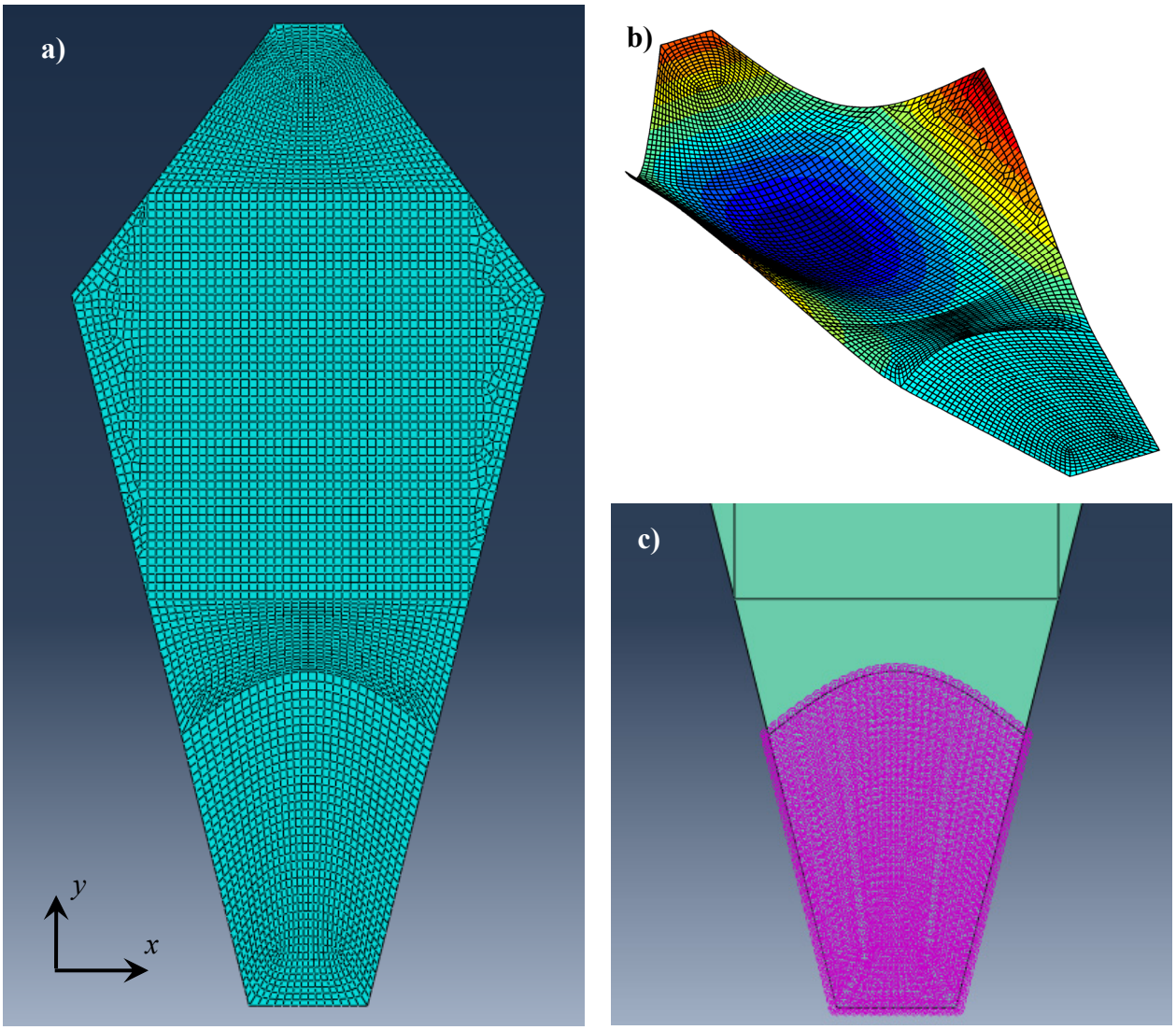

Figure 3. (a) Finite element model of the cantilevered plate (b) deformed shape of the structure in the "two-stripe" mode of interest (c) nodes where translational springs are added out of plane to simulate the clamped boundary condition.

The specimen was mounted in a clamp attached to a 12,000lb shaker with an accelerometer used to monitor the level of base excitation and a laser vibrometer measuring the response at the right wing tip. First a low level modal test was performed using random excitation and the resulting spectrum was used to estimate the natural frequencies and damping ratios of as many modes as possible. Most of the modes below 2kHz were extracted as well as a few of the modes between 2 and 3kHz and it was decided to focus model updating efforts on Modes 1-3 and 6-14. The mode shapes of the first 12 modes of the initial FE model (denoted t0 in Table 1) are shown in Fig. 4. As shown in Table 2, the natural frequencies were found to agree quite well with the FE model, with errors of less than 2-3% for most modes, although the first mode differs by almost 8%.

The model was updated using the following cost function to weight the error in each mode on a percentage basis.

$$g(\mathbf{p}) = \sum_{r=1}^{12} \left(\frac{f_{FE}(\mathbf{p}) - f_{ex}}{f_{FE}(\mathbf{p})} \right)^2 \tag{4}$$

The updating was achieved by using finite differences to compute the Jacobian of the natural frequencies with respect to each of the parameters $\mathbf{p}=[E,\nu,k]$. However, because the uncertainty on k was so large (it was not

physically derived but simply chosen to simulate the nearly fixed boundary condition), it was treated separately. Specifically, the spring stiffness was varied between 20 and 2e5 lb/in and the natural frequencies of the model were calculated and stored in a look-up table. Then for each value of k the Jacobian with respect to the other parameters $\mathbf{p}=[E,\nu]$ (at the nominal value of k) was used to compute the optimal values of $[E,\nu]$.

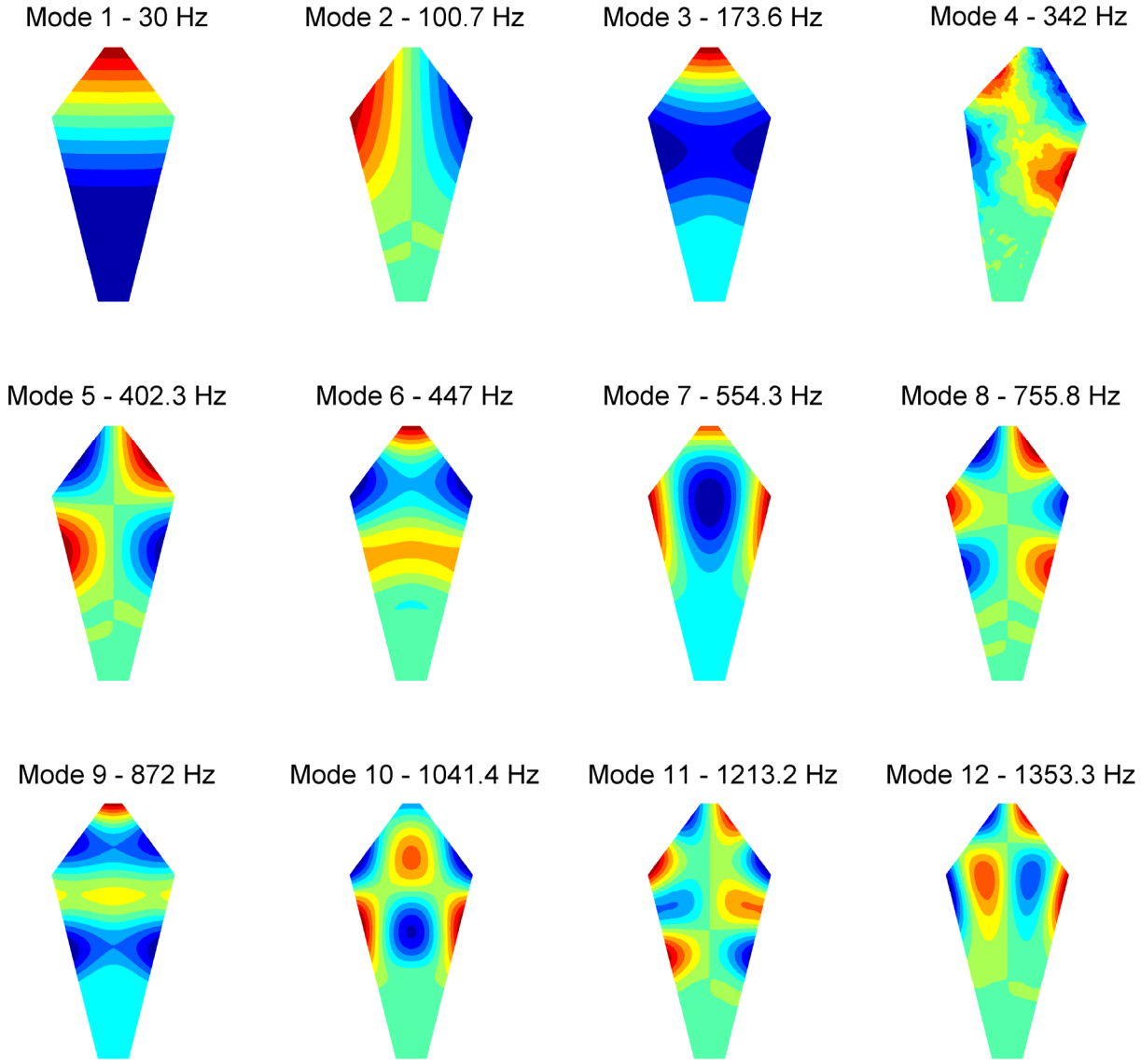

Figure 4. Mode shapes of the first twelve modes of the plate using the initial model parameters denoted t0 in Table 1.

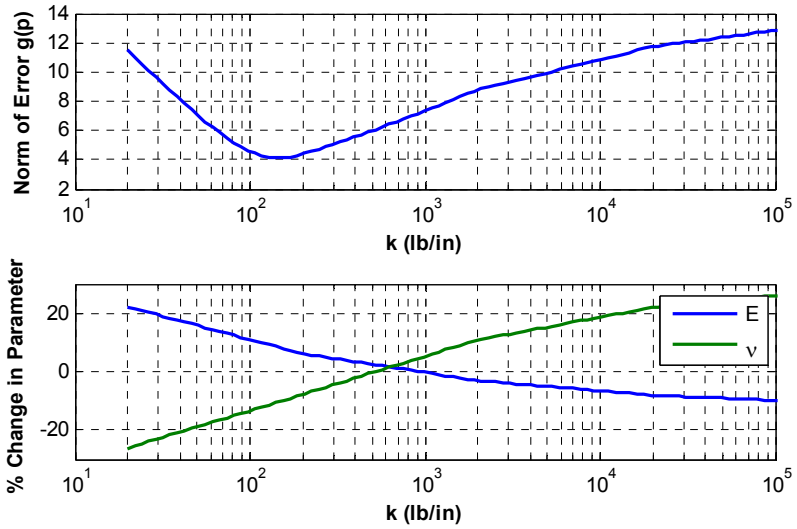

Figure 5. Optimization of the Young's modulus, *E*, and Poisson's ratio, ν, for the cantilevered plate. The nominal values for the parameters were *E*=16.5 Msi, ν=0.325 and k=2000 lb/in.

The results of the optimization, shown in Fig. 5, reveal that there are two potentially valid choices for the model parameters. One could select the value of k=141 lb/in that minimizes the cost function Eq. (4) or one could select a value of k=625 lb/in in order to keep E and ν as close as possible to their nominal values. In the literature, tests have found ν for this material to vary between only 0.32 and 0.33 and the modulus to vary between 16.5 and 18 Msi, so it may not be reasonable to change them by tens of percent. As a result, two optimized models were created, denoted t1 and t2 respectively, one with k=141 lb/in to minimize the cost function and another with k=625 lb/in to minimize the change in E and ν. The FE model was used to recompute the natural frequencies for each of these cases and the cost function, g(p), was found to be within 0.3 of the value predicted in Fig. 5 (based on the Jacobian). The natural frequencies and errors for each of these optimized models are shown in Table 2. While either is an improvement relative to the baseline model, each shows a different tradeoff in the errors of the various modes. Of particular note is Mode 7, the two stripe mode of interest, and Mode 9, which was later found to influence Mode 7 significantly. Model t1 captures Mode 7 very well at the expense of increased error in Mode 9, while Model t2 does the opposite.

Table 2: Experimental and FE natural frequencies for models denoted t0, t1 and t2.

	Natural Frequencies (Hz)						
Mode	**Exper.**	**FE t0**	**% Err t0**	**FE t1**	**% Err t1**	**FE t2**	**% Err t2**
1	27.72	29.96	8.1%	28.42	2.5%	29.33	5.8%
2	98.6	100.7	2.2%	99.5	1.0%	99.3	0.7%
3	167.9	173.6	3.4%	169.7	1.1%	171.2	1.9%
6	437.6	447.0	2.1%	437.0	-0.2%	440.8	0.7%
7	566.0	554.3	-2.1%	567.7	0.3%	558.6	-1.3%
8	756.9	755.8	-0.1%	754.0	-0.4%	749.2	-1.0%
9	861.1	872.0	1.3%	848.1	-1.5%	860.1	-0.1%
10	1041.3	1041.4	0.0%	1048.6	0.7%	1040.0	-0.1%
11	1206.5	1213.2	0.6%	1188.8	-1.5%	1198.1	-0.7%
12	1378.5	1353.3	-1.8%	1370.6	-0.6%	1365.5	-0.9%
13	1408.4	1404.3	-0.3%	1396.4	-0.9%	1387.7	-1.5%
14	1608.9	1619.4	0.7%	1607.5	-0.1%	1610.4	0.1%

Next, the nonlinear behavior of each of these models was compared by constructing an implicit condensation (IC) reduced order model (ROM) of each. After some investigation, some of which is detailed in [14], a reduced order model that included modes 1, 3, 6, 7, 9, 10, 12 and 29 was found to most effectively describe the nonlinear response of the structure below about 1000 Hz. The analysis also revealed that applying forces that would displace each linear mode 10, 3, 1, 2, 1, 1, 1 and 0.001 times the thickness seemed to provide a good balance between exciting the geometric nonlinearity sufficiently to determine the ROM coefficients while avoiding very large forces, which might introduce ill conditioning. A few of the NNMs of the plate, estimated from these ROMs, are shown in Figs. 6 and 7.

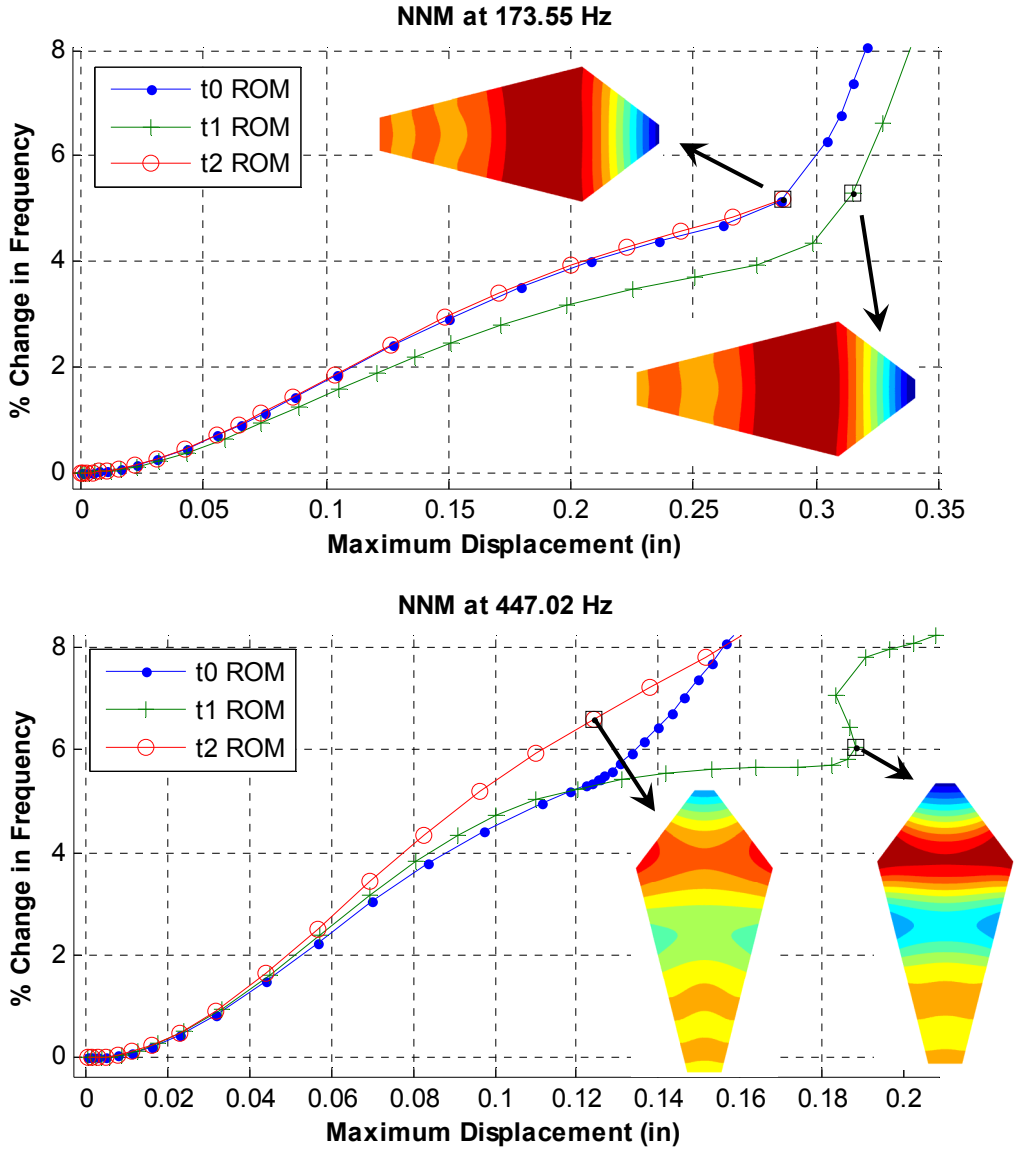

Figure 6. Nonlinear normal modes 3 and 6 of the plate for each of the finite element models. The contour plots show the initial z-displacement in each NNM for the points indicated.

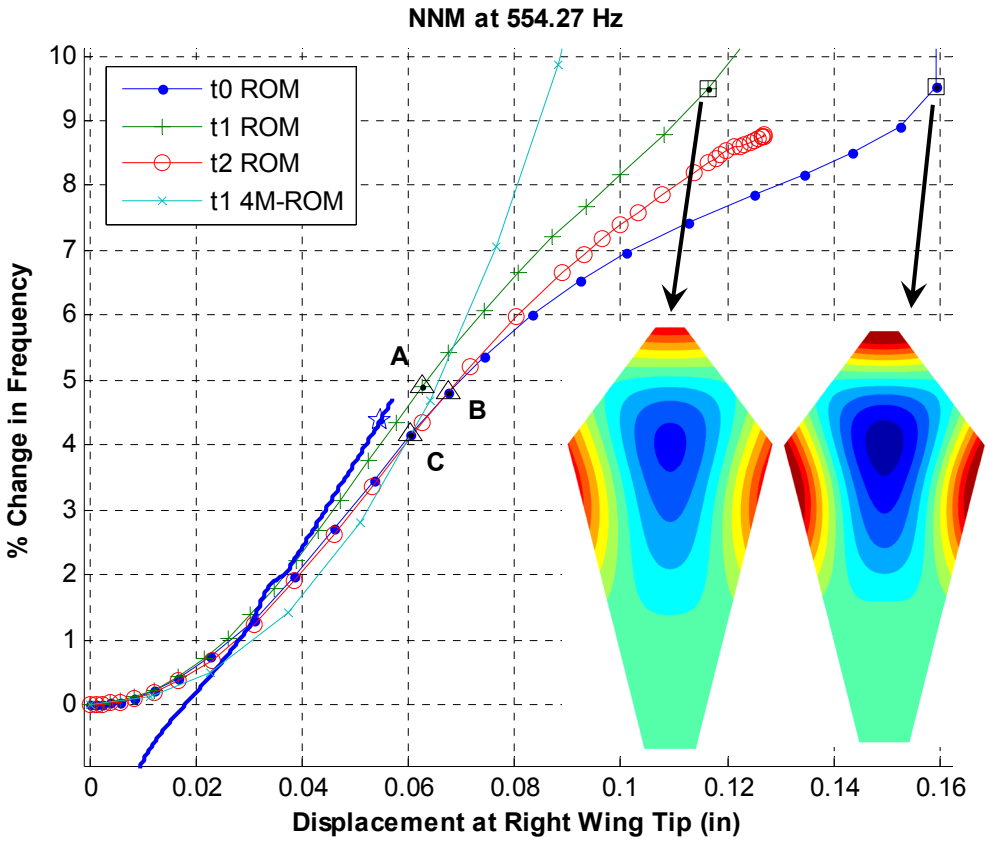

Figure 7. Nonlinear normal mode 7 (two stripe mode) of the plate for each of the finite element models. The solid blue line shows the amplitude and frequency of a sine sweep performed on the actual specimen using a base excitation of approximately 80g. The pentagram indicates the location where the response was 90 degrees out of phase with the excitation.

The NNMs reveal that bending modes 3 and 6 exhibit measurable nonlinearity as the displacement approaches between one and two times the plate thickness (0.0511 in). The two stripe mode exhibits 2 to 4 times as much nonlinearity at the same displacement. The results show that the different ROMs (and hence the different finite element models t0, t1 and t2) all show similar behavior for very small shifts in the resonant frequency, but the displacements can vary by tens of percent between the different ROMs if the frequency shifts more than about two percent. Further investigation revealed that the different frequency-energy behavior of the ROMs primarily has to do with differences in the coupling between the various modes. This is evident when comparing the deformed shape of NNMs in Figs. 6 and 7. Not only does the scale of the displacement change, but the deformation shape (and hence the stress field) also changes, most notably in case of NNM 6 but there are subtle changes in all of the shapes.

To explore this further, the time histories of NNM 7 at the points indicated in Fig. 7 for the t0 and t1 ROMs are shown in Fig. 8. (Recall that the coordinates of the ROM are the amplitudes of the linear modes included in the ROM. For this plot the modes are rescaled to a maximum value of unity so the displacements shown are in inches.) Both time histories are dominated by linear Mode 7, as one might expect, but it interesting to note that Mode 9, which is the second most significant contributor, has an opposite effect in the two different ROMs. In the t0 ROM it moves in concert with Mode 7 so the total deformation is the sum of the two shapes, while in the t1 ROM the two shapes cancel. Mode 9 is a 3rd bending mode, so this has the effect of changing the deformation of the tip of the plate relative to that of the wing tips. Mode 12 is also much more active in the t1 ROM. Finally, to further quantify the importance of modal couplings in this NNM, the frequency-displacement behavior of a fourth ROM (denoted t1 4M ROM) is also shown. This ROM includes only modes 1,3,6 and 7 for the t1 finite element model. This ROM is far stiffer at high displacement amplitudes for the same wingtip displacement and gives an idea of how much error might be incurred if the coupling between Mode 7 and the higher modes was completely neglected.

Several high amplitude sine sweeps were performed in an effort to validate the measurements for NNM 7 and one of them is shown in Fig. 7. The change in the response frequency relative to the measured linear natural frequency is plotted as if it were the "% Change in Frequency". As the frequency of the excitation changes, the phase of the response changes relative to the force. According to theory [7, 9], the resonant response is well approximated by the NNM at the point where the response is 90 degrees out of phase with the force. This point is shown with a pentagram in Fig. 7. Hence, the true NNM for this structure should be above the solid blue line and should intersect it at the point marked with a star. Model (and NLROM) t1 comes closest to the swept sine measurements, so while linear updated might have equally favored models t1 and t2, we would select model t1 based on the first nonlinear updating step. It also appears that the model should be tuned further to accurately capture the nonlinear behavior of the plate in the vicinity of this NNM. Unfortunately, without further information it is difficult to guess how the model should be changed to obtain the desired frequency-displacement behavior, so nonlinear updating will cease for this model. If more accuracy were desired then it seems that the nonlinear coupling between modes 7, 9 and perhaps 12 should be further enhanced, but with a measurement at only one point it is not possible to determine how much of each of these modes is present in the motion.

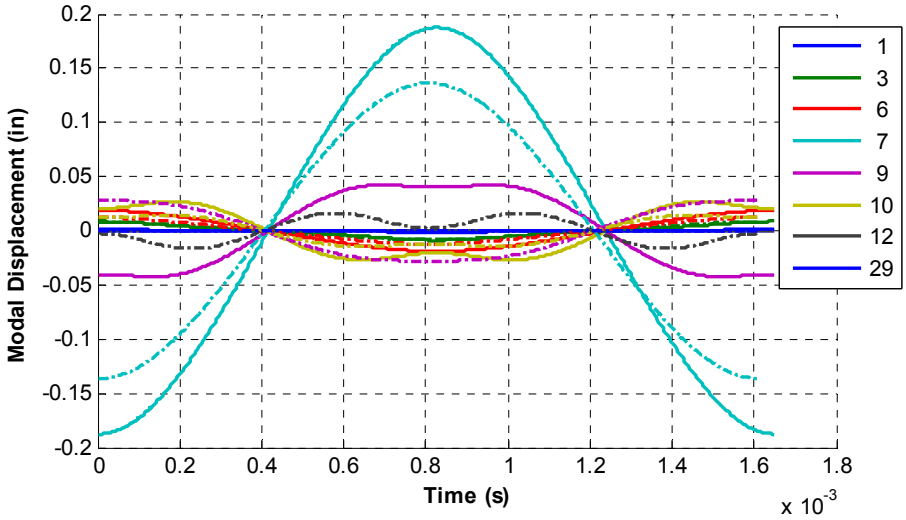

Figure 8. Displacements as a function of time for each of the modal coordinates for NNM 7 at the two points indicated with black squares in Fig. 7. (solid line = t0, dashed line = t1)

In order to relate the differences in the ROMs to the life of the plate, the solutions at the points marked with black squares in Fig. 7 were applied to the full finite element model and the stresses and strains in the part were computed. The von Mises stress from this computation, which corresponds to the state where the stress is highest over the vibration cycle, is shown in Fig. 9. It is interesting to note that the peak stress of 71ksi for the t0 model is almost twice as large as that for the t1 model (42ksi). This could translate into a difference of more than an order of magnitude in the fatigue life predicted by the two models. It is also interesting to see that the region where the point of largest stress occurs is different between these two models. The ultimate tensile strength of this type of Titanium is reported as 135-143ksi in MIL-HDBK-5H, so a response at this level might represent an extreme event but the parts are not likely to be designed to routinely reach stresses this high.

As discussed earlier, the test articles used in this work only reached about a 5% shift in the resonance frequency (under an 80 g base excitation). To illustrate the ROM predictions near that case, the stress that the part experiences when vibrating in the NNM at each of the three points marked with triangles was also computed and the results are compared in Fig. 10. If we compare the ROMs for the same shift in resonant frequency, e.g. points marked A and B in Fig. 7, then we see that the stress field differs noticeably between the two ROMs and that the maximum stress for the t0 ROM is 7.2% larger. Such a comparison is meaningful if the structure is known to experience a certain frequency shift in operation and the ROM seeks to capture that. If we instead compare points A and C, where the maximum displacement at the wing tip is approximately equal, then the t0 ROM predicts a 7.4% lower stress than the t1 ROM. This comparison would be meaningful if the part was known to experience 0.06 in of displacement at the wing tip. It is important to note that these two ROMs would not necessarily reach equal maximum displacements when subjected to the same force. Because the system is nonlinear one must integrate the ROM to

compute the response to a given loading, and that response could involve all of the modes of the structure. But the force required can be estimated using the method in [15]. Using that approach and assuming that the damping is fixed and modal, described by the low-level damping ratios that were measured, we find that to excite the observed NNM motions using a sinusoidal point force at the right wing tip, force amplitudes of 0.197 lb, 0.199 lb and 0.172 lb would be required for points A, B and C respectively. The ROM can be integrated with this forcing to verify that these values are quite accurate.

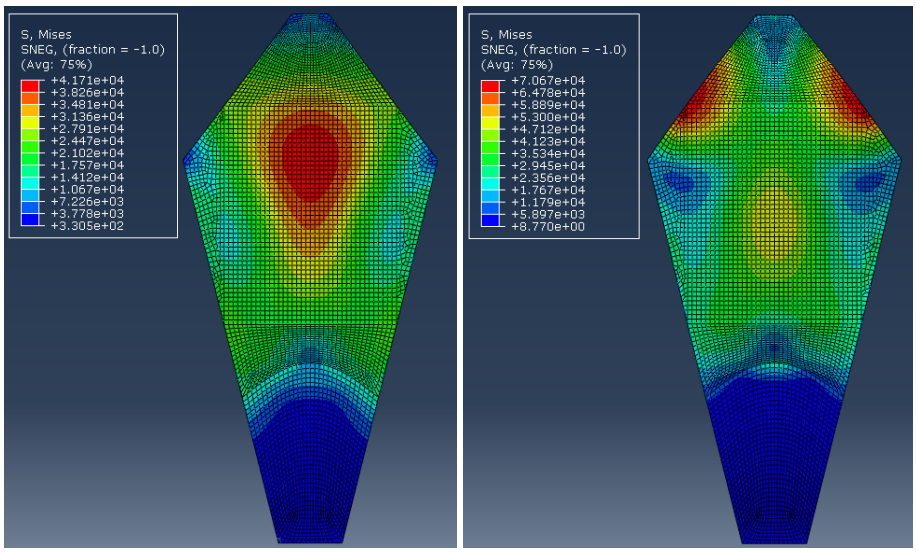

Figure 9. Maximum von Mises stress in the plate when vibrating in NNM 7 at the two points indicated with black squares in Fig. 7. (left = t1, right = t0)

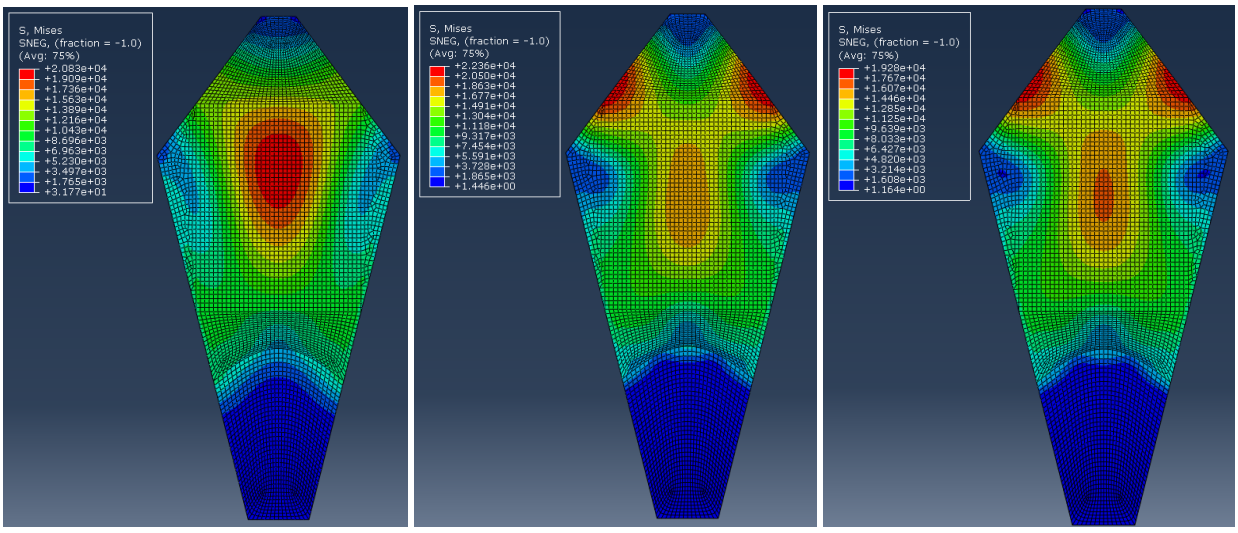

Figure 10. Maximum von Mises stress in the plate when vibrating in NNM 7 at the three points indicated in Fig. 7. (left = t1-A, middle = t0-B, right = t0-C)

IV. Panel from Lynx Helicopter

The second system studied is dramatically more challenging than the cantilevered plate. The linear dynamics are more complicated due to the curvature, geometry and material properties, and the nonlinear response of the panel will probably depend strongly on the stiffness of the frame and hence nonlinear updating will be critical. No drawings were provided by the manufacturer, so the panel model was developed empirically. A set of measurements was acquired with a ruler and the plate profile was measured by tracing the curved edge onto graph paper. The authors also used the Kinect™ system described in [11] to measure the geometry over a cloud of points and a visualization of this measurement is shown in Fig. 11a. This data provided a useful reference and sanity

check. The Kinect also makes it possible to account for the difference between the angle at which the measurement is taken relative to the surface and the surface normal. In the end a quadratic function $z = 0.00234y^2 - 0.798y + 68.4$, was found to describe the profile well. A mesh of shell elements was created in Matlab®, defined parametrically to allow optimization of the mesh and geometry, and then used to write input scripts for Abaqus, which was used to perform all FE analyses. The stiffeners at the back of the panel were approximated with one-dimensional beam elements, fixed to the shell in all relevant degrees of freedom with an offset equal to half their thickness. The shell mesh is shown in Fig. 11b, and the corresponding beam mesh is overlaid on the relevant nodes; the offset between the neutral axis of the beam and their connection to the shell elements was accounted for but is not represented in this simple figure. The model had a total of 20,116 nodes.

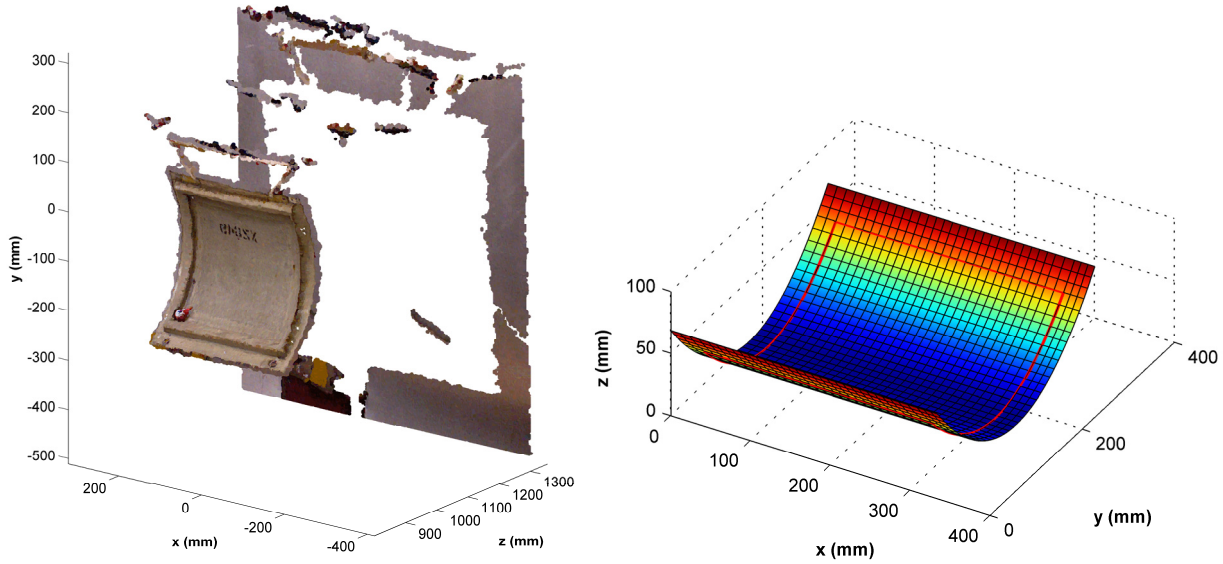

Figure 11. Point cloud generated by Kinect (left) and finite element mesh generated for the plate (right).

A. Linear Model Updating

The green line in Fig. 12 shows a composite (i.e. average over all of the measurement points) of the frequency responses measured on the panel using a low-level, broadband random excitation at the location shown in Fig. 1. The panel was then moved into a sound absorbing room and swept sine tests were performed at various amplitude levels. Figure 12 also shows a few sample results from those tests. Comparison shows that several of the modes of the panel are noticeably nonlinear with a 2N excitation force. One of the dominant modes with this input location was the mode near 380 Hz, which exhibited a peak response of about 0.056mm at the measurement point to the 2N excitation. Note that the place where the shaker input was applied was chosen such that the shaker would not mass load or otherwise change the dynamics of the panel very much; it certainly was not optimal to excite all of the modes. The mode near 460 Hz also seems to exhibit significant nonlinearity.

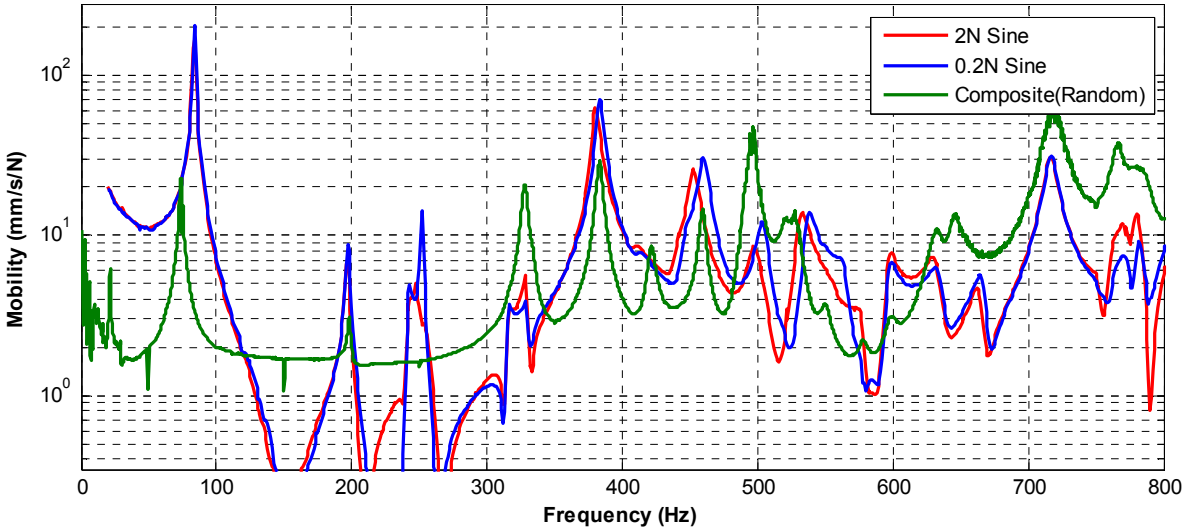

Figure 12. Frequency responses measured on the plate in two setups. In the first test (green), broadband random excitation was used and the mode shapes shown in Figs. 13 through 16 were acquired. The second test was performed with nominally identical boundary conditions using stepped sine excitation and measuring at only one point on the panel.

The initial finite element model predicted the natural frequencies of the panel within about a factor of two, but significant error checking was required to correct the model and bring it into better agreement with the measurements, especially as regarded the definition of the bending directions and material properties for the beam elements. Once these issues had been corrected the models agreed qualitatively and a few gradient-based optimization steps were then used to bring the frequencies into closer agreement. The density of the shell was assumed to be 1500 kg/m^3 and that of the beams was adjusted until the mass of the panel matched the measured mass, resulting in a density of 629 kg/m^3 for the beams. These parameters were not altered. In a first step the beam properties were adjusted to bring modes 1 and 2, which were dominated by the beam stiffnesses, into close agreement. These modes were dominated by the stiffness of the beams, so it was hoped that this step would serve to identify the beam stiffness properties. Then several bending modes began to agree closely enough that they could also be considered and a second iteration was performed in which the shell modulus and thickness was also updated.

Table 3: Parameters of FE model before and after various updating steps.

Parameter	Initial Values	Update based on Modes 1 and 2	Updated based on Modes 1,2,4,6,14
I (beams)	2.3801e-09 m^4	1.1028e-09	1.792e-09
J (beams)	4.0164e-09 m^4	4.322e-10	1.3544e-09
E (shell)	17 GPa	same	9.7808e9
h_o (shell thickness outer section)	1.3 mm	same	1.4
h_i (shell thickness inside section)	1.3 mm	same	1.2

The natural frequencies of the FE model are compared with those extracted from the LDV measurements in Table 4. Several of the FEA mode shapes are compared with the operating deflection shapes measured with the LDV in Figs. 13 through 16. The comparisons show that the FE model is qualitatively quite similar for most of the first ten or so modes of the panel, but many of the modes are dominated by bending of the free edges of the panel and other small-scale features that this model doesn't seem to capture very accurately. However, the current model does seem to capture the stiffness of the frame (dominated by modes 1 and 2) and the membrane bending of the shell so it was hoped that it might be adequate to describe the nonlinear behavior of the panel.

Table 4: Natural frequencies of FEM and measured in SLDV test.

Elastic Mode	FE Model	Measured	Description
1	73.768	74.06	1st torsion
2	193.96	198.13	1st bending
3	305.21	-	(3,1) lobe membrane
4	305.47	-	2nd Torsion
5	315.92	327.5	(2,1) lobe membrane
7	367.79	383.13	(4,1) lobe membrane
8	442.22	-	(4,1) lobe memb. + 3-node bottom edge
	-	459.38	(4,1) lobe memb. + 2-node bottom edge + 2-node top edge in phase
		521.5, 527.5	3-node bottom edge
14	581.63	578.44	(4,2) lobe membrane
		598.75	(4,2) lobe memb. + 4 node bottom edge

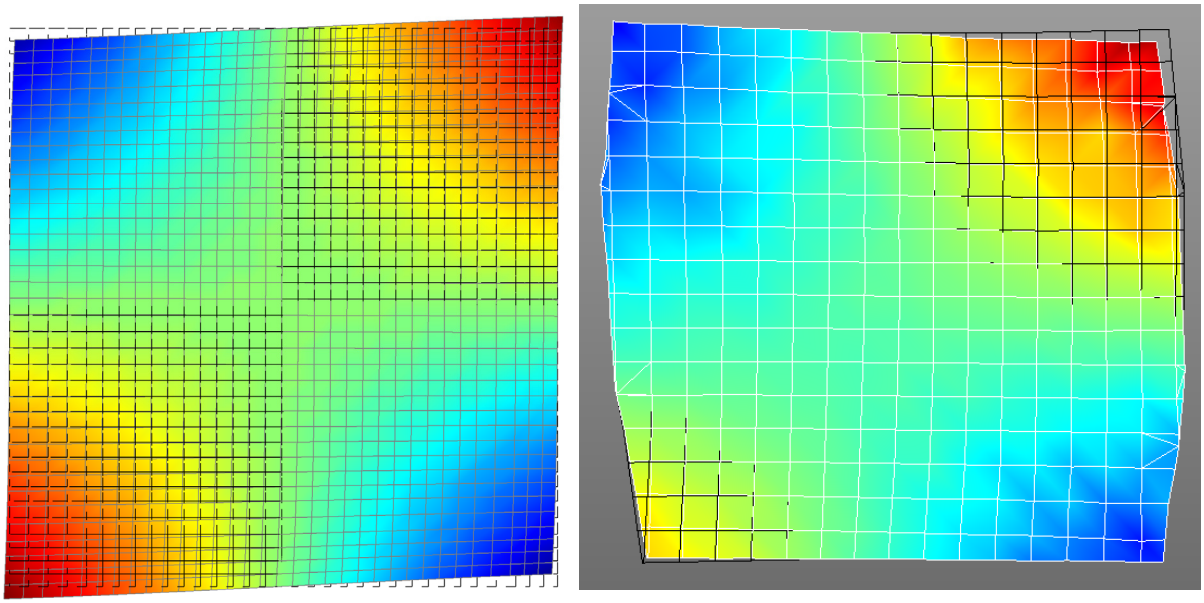

Figure 13. First mode from FEM at 73.77 Hz (left) and test at 74.06 Hz (right).

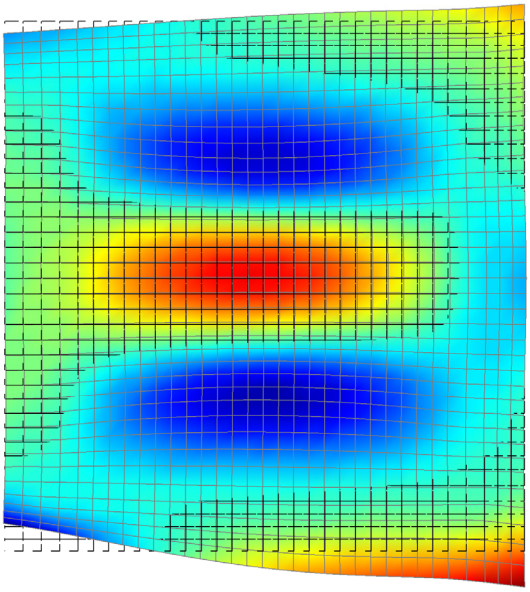

Figure 14. Mode 3 from FEM at 305.21 Hz

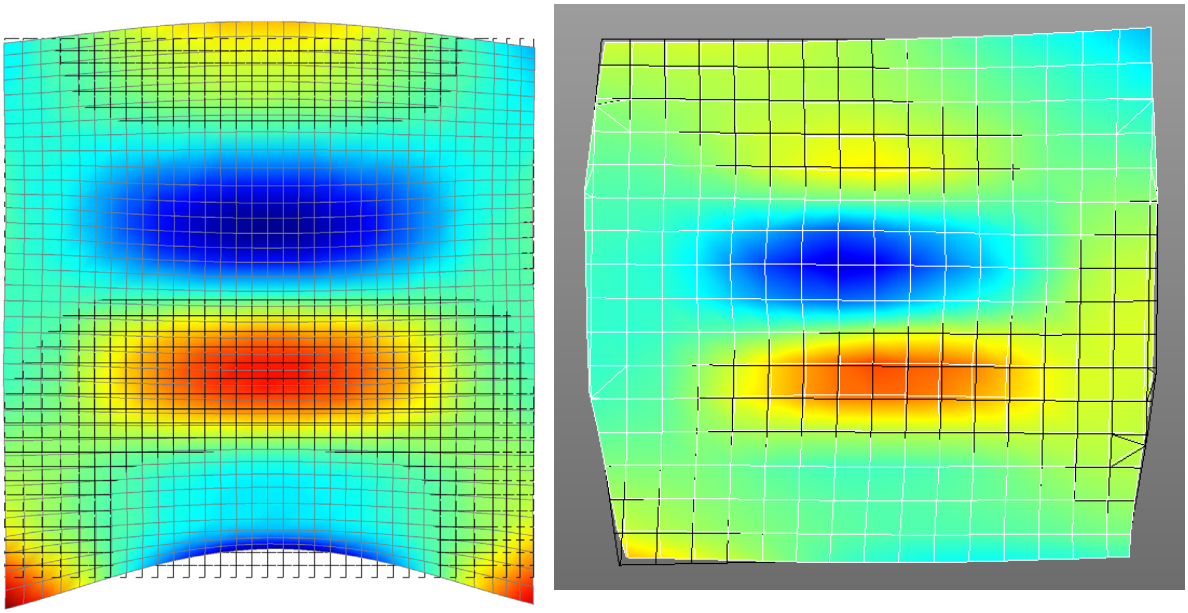

Figure 15. Mode 5 from FEM at 315.9 Hz (left) and test at 327.5 Hz (right).

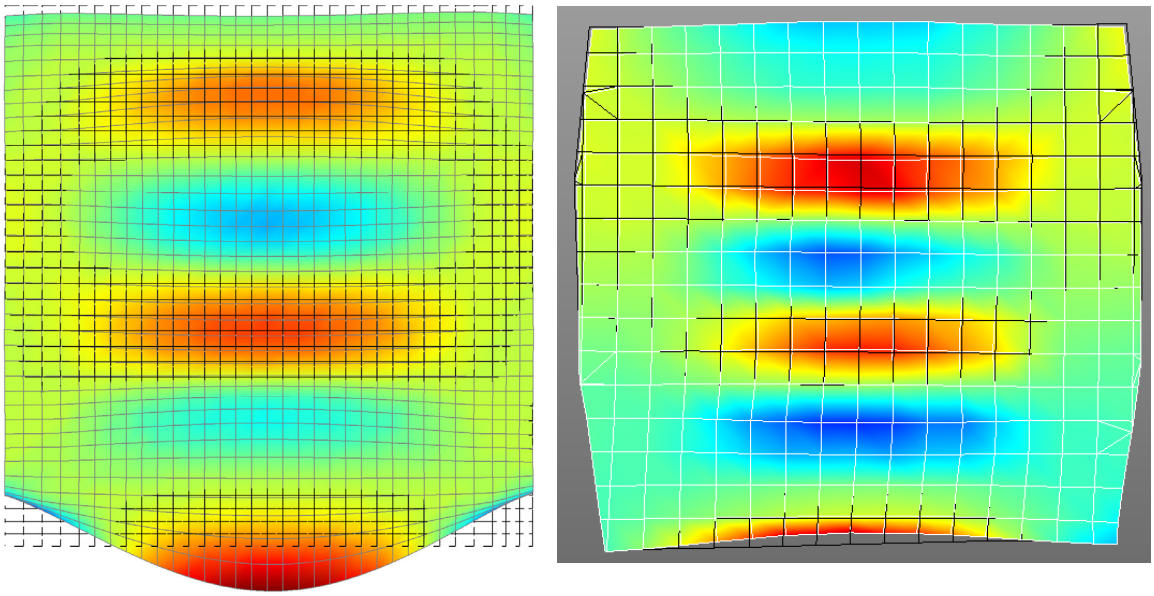

Figure 16. Mode 7 from FEM at 367.8 Hz (left) and test at 383.1 Hz (right).

B. Nonlinear Modeling

Several reduced order models of the panel were created using the ICE method described in [12, 13]. Because this structure has free boundary conditions, the approach had to be modified slightly. Specifically, the constraint $\boldsymbol{\varphi}_{RB}{}^{\mathrm{T}}\mathbf{M}\mathbf{x} = 0$ was applied as six multi-point constraints[3] where $\boldsymbol{\varphi}_{RB}$ contained the six rigid body modes of the panel, **M** is the mass matrix and **x** the vector of displacements of all of the nodes in the FEA model. This preserves all of the elastic modes while constraining away rigid body motion. Then, the FEA model was deformed statically using a load that would excite only the 5th (315.9 Hz) linear mode at small force levels. For larger loads, this static force also excites modes 2, 6, 7 and 9 due to nonlinear coupling, so those modes were included in a ROM.

Because of the way in which the constraints $\boldsymbol{\varphi}_{RB}{}^{\mathrm{T}}\mathbf{M}\mathbf{x} = 0$ were implemented, the cost of computing the static response of the constrained model was substantial (over ten hours were required to estimate a ROM). Hence, there was only time to create about five different ROMs and of those the case that was thought to be most accurate was the case where modes [2,5,6,7,9] were displaced, respectively, by forces that would cause a linear deformation of [0.5, 0.2, 0.5, 0.5, 0.2] times the thickness. The resulting nonlinear deformations ranged from 0.2 to 0.8 times what was expected for the linear model, so these loads are somewhat larger than the optimum suggested in [5]. The NNMs computed from these load cases are shown in Fig. 17. Two curves are shown for each NNM corresponding to the case where the ROM is computed using a "constrained" fit (where certain symmetries are enforced) or "unconstrained" as explained in [5, 12]. The unconstrained fit was found to capture the static load cases more accurately; the norm of the difference between the static loads and those predicted by the ROM was 0.03 for that fit as opposed to 0.07 for the constrained fit, but in any event the two curves for each mode give some indication of the level of uncertainty that is present in the ROMs. For modes 5 and 9, a maximum deformation of 1-2 millimeters is expected to correspond to a 1% shift in the natural frequency, and more than a 5% change in frequency is expected if the deformation exceeds 4-5 mm. The panel is not likely to survive larger deformations for an appreciable amount of time, but the exact stresses that the panel would experience at these deformation levels are not yet known.

The simulations also reveal that the deformation shape of the structure is strongly dependent upon the response level. For example, the deformation shape of NNM 5 is shown in Fig. 18 for both a linear deformation and for the two energy levels indicated in Fig. 17. As energy increases the deformation is predicted to localize to the bottom edge of the panel. This phenomenon is likely to be quite sensitive to the panel thickness on the edge and to the way

[3] The authors later discovered that this set of constraints destroys the bandedness of the matricies, causing a large increase in the memory requirements and computational cost. The Abaqus documentation suggests an alternative where one can avoid this by replacing these six equations with many equations involving additional variables, each having a much smaller number of terms. The authors have not yet implemented that approach.

in which this part is joined to the frame and so the current model may need to be improved to reproduce this behavior.

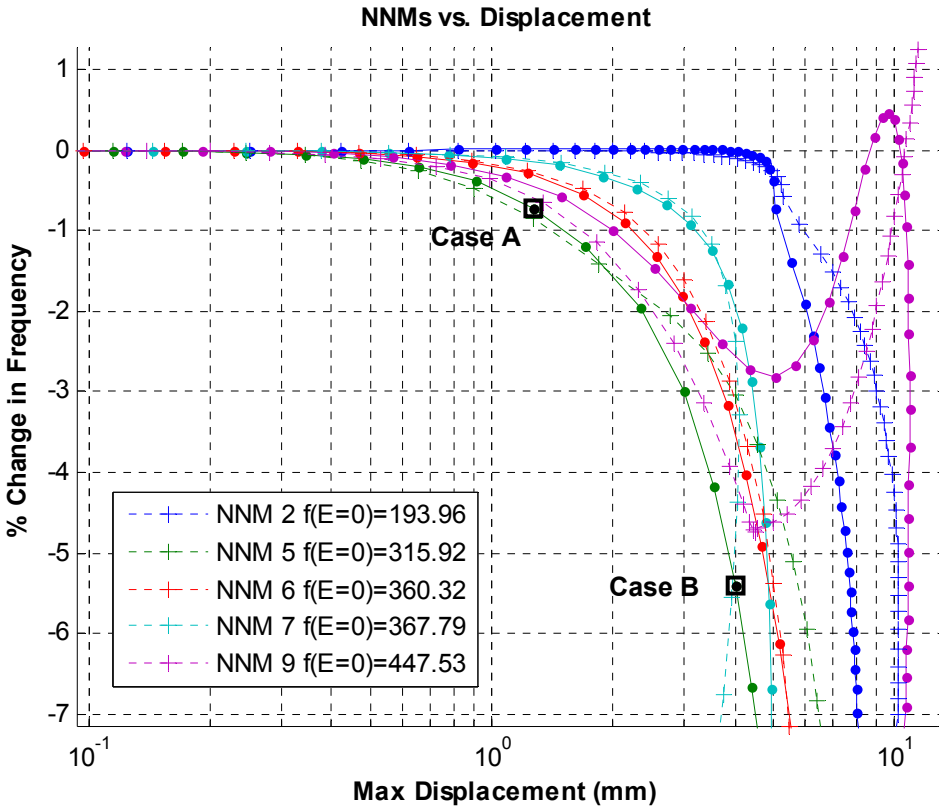

Figure 17. Nonlinear normal modes computed from a 5-mode reduced order model of the panel.

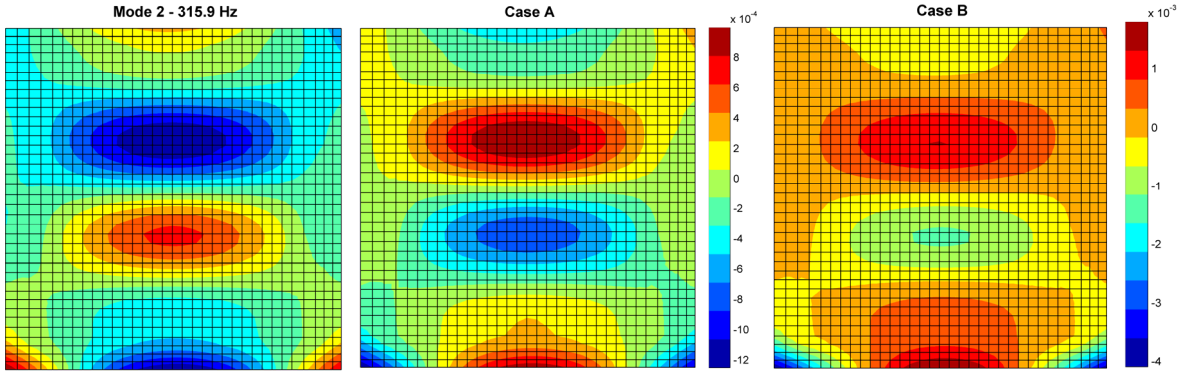

Figure 18. Deformation shapes of the 5th NNM (315.9 Hz at low amplitude) for the cases indicated in Fig. 17. The peak displacement is -1.2mm in Case A and -4mm in Case B.

C. Nonlinear Testing

A sequence of stepped-sine tests was performed near a few of the resonances that exhibited the most nonlinearity to extract the nonlinear mode backbone. For example, the stepped sine measurements near the 460Hz resonance are shown in Fig. 19. A closed-loop control algorithm was used to adjust the signal sent to the shaker at each frequency line in order to assure that the input force was a sinusoid (to 99% tolerance) at the desired level. Typically, the algorithm had to increase the drive voltage to the shaker by an order of magnitude near resonance to achieve this objective, and a few harmonics of the drive signal had to be adjusted to produce a sinusoidal force.

The measurements show a softening nonlinearity, where the peak of the resonance decreases about 10 Hz as the input amplitude increased by a factor of 50. The NNMs was extracted from these measurements by identifying the point at which the response was 90 degrees out of phase with the force and the displacement versus frequency is shown in Figs. 20 and 21. The measurements show that the nonlinearity becomes significant as the displacement approaches 0.01mm, which is about an order of magnitude smaller than what is predicted by the reduced order models. The reason for this is not known, but perhaps it should not be too surprising since the finite element model only roughly reproduces the modes of the panel. The results of this exercise suggest that one might need quite an accurate model for a panel such as this to accurately reproduce the nonlinear behavior, although it is perhaps encouraging to see that the model used here gives near the correct order of magnitude.

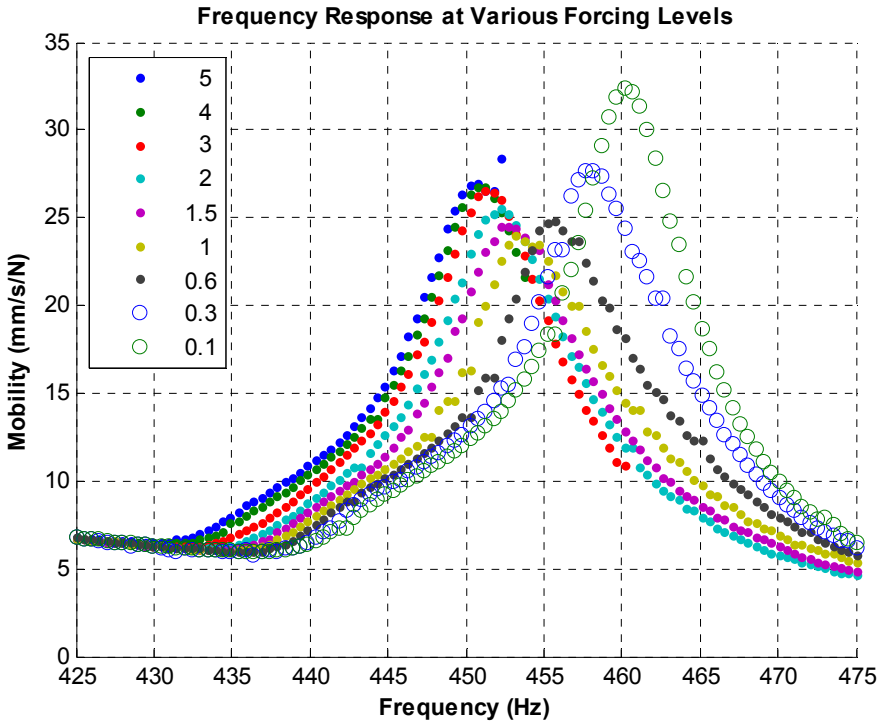

Figure 19. Experimentally measured response near the 460 Hz resonance.

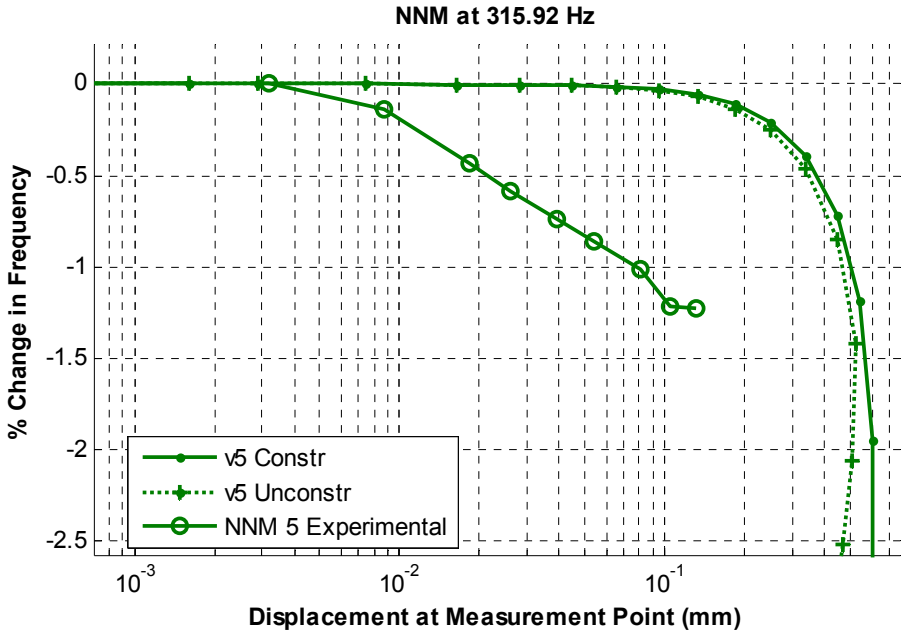

Figure 20. Comparison of the frequency-displacement behavior of the measured 5th NNM and that predicted by the finite element model.

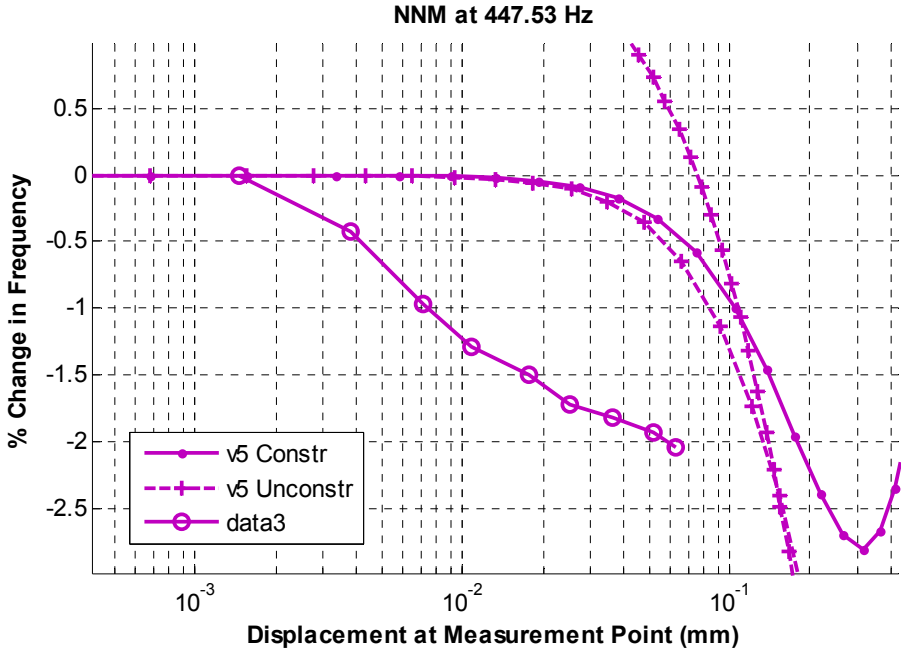

Figure 21. Comparison of the frequency-displacement behavior of the measured 9th NNM and that predicted by the finite element model.

The simulation results show that the behavior of each nonlinear mode depends strongly on how the underlying linear modes couple as the force amplitude increases. This behavior cannot be experimentally corroborated unless measurements are taken at many points on the surface. This was pursued in this work using Continuous-Scan Laser Doppler Vibrometry [16-18]. Because the desired excitation was sinusoidal and a measurement with very high resolution was desired, the methodology outlined in [11] was employed. Specifically, the scan pattern consisted of two slow sinusoids with 7.5 cycles/minute and 7.6 cycles/minute in the vertical and horizontal directions respectively. Using this pattern, the laser covers the surface densely over the 10 minute measurement window, as shown in Fig. 22. During initial tests the panel was mounted in an acoustically insulated booth and the laser imaged

the surface through a window as shown in the upper picture in Fig. 22. However, spurious reflections from the laser on the glass caused considerable noise and measurement artifacts. Eventually this setup was abandoned and the vibrometer and panel were mounted together within the booth as shown in the lower picture.

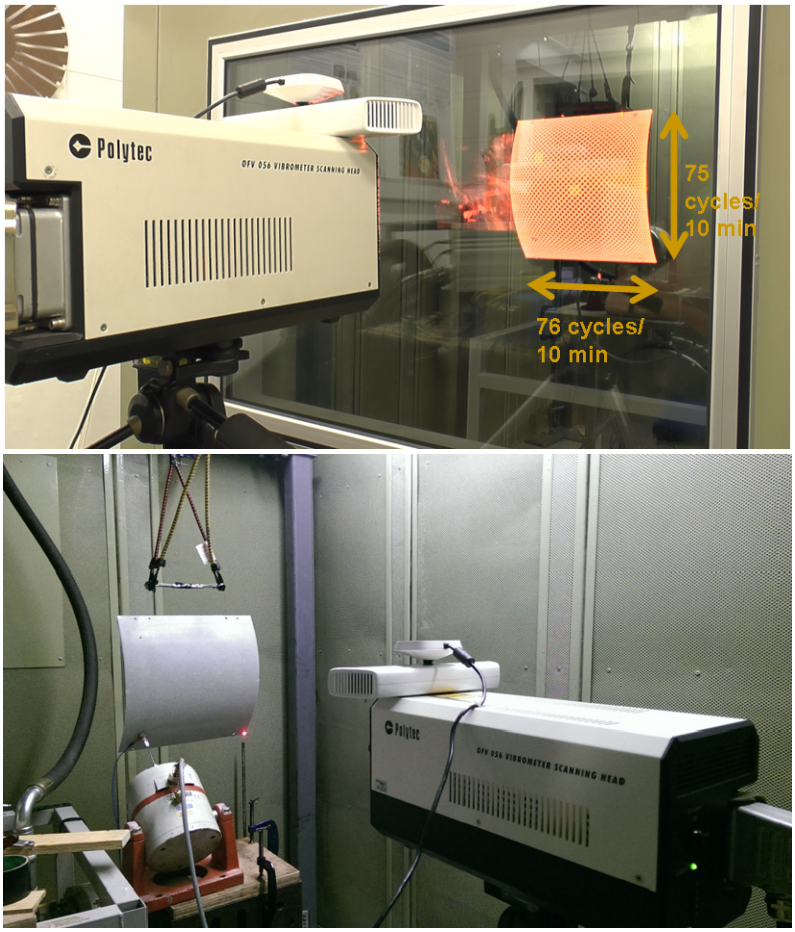

Figure 22. Photographs of initial (top) and final (bottom) setup for CSLDV measurements.

Figure 23 shows the response of the panel in this configuration to a stepped sine near 460 Hz. The response now shows two peaks near this frequency. For these measurements the panel was excited from the front (see Fig. 22) and with a larger shaker than was used in the earlier tests. Also the suspension system was changed replacing elastic cords with fishing line. Presumably these changes have altered the system slightly so that two modes are now excited.

Figure 24 shows example ODSs from the CSLDV scans, taken at various frequencies and force levels, trying to follow the resonant backbones of the two modes as best as possible. As a first approximation, the low-level ODSs were taken as estimates of the mode shapes (which was straightforward since the modes were well-separated in frequency at low force levels). These shapes were also correlated against the ODSs measured at higher force levels to explore the mixing between the shapes as amplitude increased. The correlation was performed using a normalised vector inner-product (e.g. the modal assurance criterion, MAC between the shapes). The correlation of mode A with itself is seen to reduce as the forcing level was increased, whilst the correlation of mode A with mode B is seen to increase as the forcing level increased. The same can be said of mode B. This is unsurprising, since the resonances converge at higher force levels, and so the ODS becomes a combination of two modes with similar energy levels. A plot such as this is expensive in terms of testing time, and is experimentally difficult. It was not trivial to accurately track the backbones nor to minimize the higher harmonics in the forcing signal. However, significant insight into the coupling between these modes is clearly made possible. In the lower frequency mode the deformation is localized to the bottom edge of the panel, while the higher frequency deformation shape resembles a (4,1) lobe membrane mode. These shapes are denoted Mode A and Mode B. The frequency of Mode A remains

essentially constant, as one might expect for a mode that involves little membrane stretching. In contrast, the frequency of Mode B drops, and as it drops its shape seems to take on more of the character of Mode A. The behavior observed here is qualitatively similar to what the FEA model predicted for the modes near 315 Hz, as was illustrated in Fig. 18.

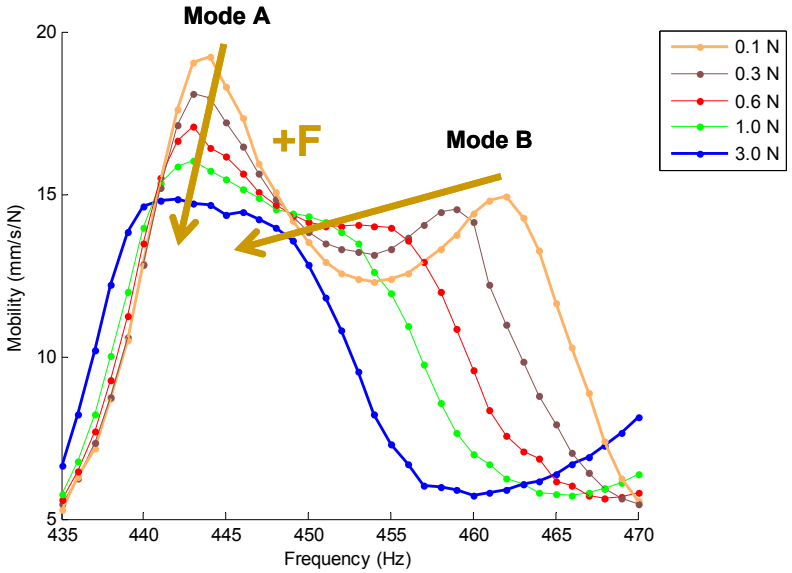

Figure 23. Photographs of initial (top) and final (bottom) setup for CSLDV measurements.

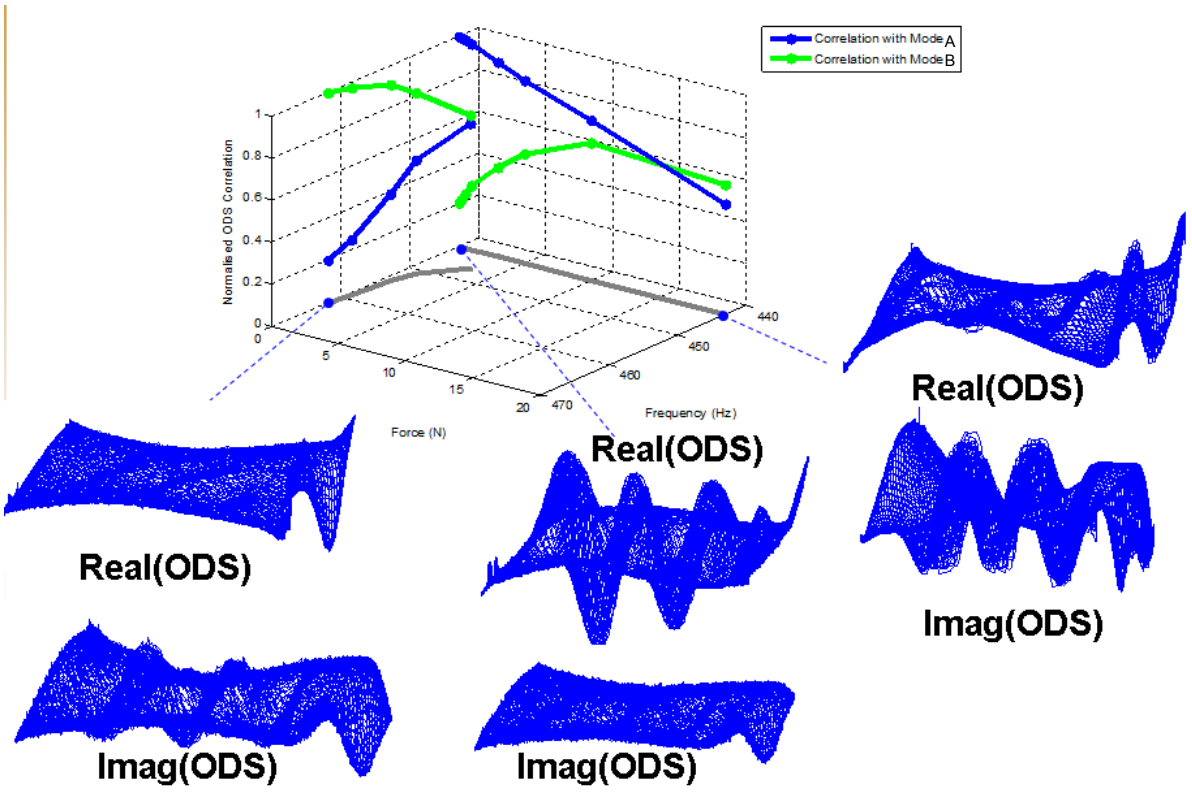

Figure 24. Summary of operating deflection shape measurements with CSLDV. Two distinct shapes seen at low force levels, are denoted Mode A and Mode B. As the forcing amplitude increases the ODS changes becoming a linear combination of these shapes.

D. Discussion

The experimental campaign has confirmed that it is feasible to compute the frequency-energy behavior and the deformation shapes of a nonlinear panel with sufficient fidelity to understand the modal interactions that drive the nonlinear behavior. Unfortunately, the FEA model is currently not of sufficient quality to be brought into close agreement with the measurements but with sufficient resources to collect additional measurements and more modeling effort it does appear that model updating based on nonlinear normal modes is feasible even for a fairly complicated structure such as this. If the CAD geometry for the panel had been available and more was known about its construction the results would likely have been improved.

V. Conclusions

This work has sought to assess the suitability of nonlinear modeling, testing and model updating for geometrically nonlinear structures. Two structures were considered, the first being a flat cantilevered plate that was relatively simple and a model was developed that very accurately captured the linear behavior and the nonlinear behavior up to relatively large energies, at least insofar as could be determined based on measurement data that was available. The comparisons revealed that spatially detailed measurements would be needed to validate/update the model at higher energies, as the nonlinear behavior begins to depend on which linear modes interact.

The second structure considered, a skin panel from a Lynx helicopter, posed a much more significant challenge. Because little was known about the construction of the panel significant updating was needed to obtain a model and the in time available for the project it was only possible to create a relatively crude model. Furthermore, the curved structure exhibits rich dynamics with both softening and hardening nonlinearities and even more complicated interactions between the underlying linear modes. An experimental campaign involving stepped sine testing and continuous-scan laser Doppler vibrometry showed that it is feasible to obtain highly detailed measurements that reveal how the deformation shape changes with increasing amplitude; measurements such as these may be the key to determining whether the nonlinear model accurately represents the structure of interest.

This research has also highlighted several areas where further research is needed. First, stepped sine testing is straightforward and does seem to produce high quality estimates of the nonlinear response. However, at high force levels it is difficult to achieve a sinusoidal input signal and the tests are exceedingly slow. It would be preferable to have a means of stepping directly along the NNM backbone rather than performing several sweeps near resonance and then extracting the backbone after the fact. The swept sine measurements used on the cantilevered plate were simpler to perform, and that may be an excellent alternative in many cases, especially if spatial data could be collected simultaneously.

Several challenges also remain in the modeling realm; although the reduced order modeling techniques have been used for almost two decades, there is still little guidance in the literature regarding what load levels to use and how many modes must be included to obtain a model that is valid over a desired range of loads or displacements. The authors continue to explore these issues [5, 14, 19] and as a result better rules are emerging to guide the process of generating a nonlinear ROM. All of the computations required for the cantilevered plate were easily performed on a laptop computer and none took more than a few hours. It was far more expensive to solve the static load cases for the Lynx panel, and that inhibited our efforts significantly, but if a more efficient means had been available for constraining away the rigid body modes then presumably that structure would also have been relatively easy to deal with. Once the ROMs were created the NNMs could be estimated in a few minutes, and the response to arbitrary loadings can also be computed very inexpensively.

Acknowledgments

This work was supported by the Air Force Office of Scientific Research, Award # FA9550-11-1-0035, under the Multi-Scale Structural Mechanics and Prognosis program managed by Dr. David Stargel. The authors also wish to thank Dr. Joseph Hollkamp and other collaborators in the Structural Sciences Center at the Air Force Research Laboratory for providing the Abaqus® interface that was used in this work, the test data and finite element model for the cantilevered plate and for the discussions which played a significant role in shaping this work.

References

[1] R. D. Cook, D. S. Malkus, M. E. Plesha, and R. J. Witt, *Concepts and Applications of Finite Element Analysis*, 4th Edition ed. New York: Wiley, 2002.

[2] J. J. Hollkamp, R. W. Gordon, and S. M. Spottswood, "Nonlinear modal models for sonic fatigue response prediction: a comparison of methods," *Journal of Sound and Vibration,* vol. 284, pp. 1145-63, 2005.

[3] M. P. Mignolet, A. Przekop, S. A. Rizzi, and S. M. Spottswood, "A review of indirect/non-intrusive reduced order modeling of nonlinear geometric structures," *Journal of Sound and Vibration,* vol. 332, pp. 2437-2460, 2013.
[4] R. J. Kuether and M. S. Allen, "Computing Nonlinear Normal Modes Using Numerical Continuation and Force Appropriation," presented at the ASME 2012 International Design Engineering Technical Conferences IDETC/CIE 2012, Chicago, IL, 2012.
[5] R. J. Kuether, B. Deaner, M. S. Allen, and J. J. Hollkamp, "Evaluation of Geometrically Nonlinear Reduced Order Models with Nonlinear Normal Modes," *AIAA Journal,* vol. Submitted August, 2014.
[6] R. J. Kuether and M. S. Allen, "A Numerical Approach to Directly Compute Nonlinear Normal Modes of Geometrically Nonlinear Finite Element Models," *Mechanical Systems and Signal Processing,* vol. 46, pp. 1–15, 2014.
[7] M. Peeters, G. Kerschen, and J. C. Golinval, "Dynamic testing of nonlinear vibrating structures using nonlinear normal modes," *Journal of Sound and Vibration,* vol. 330, pp. 486-509, 2011.
[8] P. J. O'Hara and J. J. Hollkamp, "Modeling vibratory damage with reduced-order models and the generalized finite element method," *Journal of Sound and Vibration,* vol. 333, pp. 6637-6650, 2014.
[9] M. Peeters, G. Kerschen, and J. C. Golinval, "Modal testing of nonlinear vibrating structures based on nonlinear normal modes: Experimental demonstration," *Mechanical Systems and Signal Processing,* vol. 25, pp. 1227-1247, 2011.
[10] R. J. Kuether, M. R. Brake, and M. S. Allen, "Evaluating Convergence of Reduced Order Models Using Nonlinear Normal Modes," presented at the 32nd International Modal Analysis Conference (IMAC XXXII), Orlando, Florida, 2014.
[11] B. Weekes and D. J. Ewins, "Multi-Frequency, 3D ODS Measurement by Continuous-Scan Laser Doppler Vibrometry," *Mechanical Systems and Signal Processing,* vol. (under review), 2014.
[12] R. W. Gordon and J. J. Hollkamp, "Reduced-order Models for Acoustic Response Prediction," Air Force Research Laboratory, AFRL-RB-WP-TR-2011-3040, Dayton, OH2011.
[13] J. J. Hollkamp and R. W. Gordon, "Reduced-order models for nonlinear response prediction: Implicit condensation and expansion," *Journal of Sound and Vibration,* vol. 318, pp. 1139-1153, 2008.
[14] R. J. Kuether and M. S. Allen, "Validation of Nonlinear Reduced Order Models with Time Integration Targeted at Nonlinear Normal Modes," presented at the 33rd International Modal Analysis Conference (IMAC XXXIII), Orlando, Florida, 2015.
[15] R. J. Kuether, L. Renson, T. Detroux, C. Grappasonni, G. Kerschen, and M. S. Allen, "Nonlinear Normal Modes, Modal Interactions and Isolated Resonance Curves," *TBD,* vol. Submitted Sept. 2014, 2014.
[16] M. S. Allen and M. W. Sracic, "A New Method for Processing Impact Excited Continuous-Scan Laser Doppler Vibrometer Measurements," *Mechanical Systems and Signal Processing,* vol. 24, pp. 721–735, 2010.
[17] M. Martarelli, "Exploiting the Laser Scanning Facility for Vibration Measurements," Ph.D. Ph.D., Imperial College of Science, Technology & Medicine, Imperial College, London, 2001.
[18] A. B. Stanbridge and D. J. Ewins, "Modal testing using a scanning laser Doppler vibrometer," *Mechanical Systems and Signal Processing,* vol. 13, pp. 255-70, 1999.
[19] L. C. M. Guerin, R. J. Kuether, and M. S. Allen, "Considerations for Indirect Parameter Estimation in Nonlinear Reduced Order Models," presented at the 33rd International Modal Analysis Conference (IMAC XXXIII), Orlando, Florida, 2015.